CrossMark

Effect of sulphur concentration on the structural and electronic properties of ZnS nanoparticles synthesized using chemical precipitation method

Harit Kumar Sharma[1] · P. K. Shukla[2] · S. L. Agrawal[1]

Abstract A systematic study is presented on the synthesis of ZnS nanoparticles by using simple chemical precipitation method without using any capping agent. The ZnS nanoparticles have been synthesized using precursor solution with different $Zn^{2+}:S^{2-}$ ratio. The as synthesized nanoparticles have been characterized by X-ray diffraction (XRD), scanning electron microscopy (SEM), atomic force microscopy (AFM), UV–Vis absorption spectroscopy and impedance spectroscopy. The XRD patterns reveal the formation of ZnS nanoparticles with wurtzite hexagonal phase which changes to sphalarite phase for higher concentration of S^{2-} in the precursor solution. XRD, SEM and AFM studies have shown enhancement in particle size on increasing sulphur content. SEM and AFM images depict formation of deformed spherical nanoparticles with particle size ranging from 10 to 50 nm. Optical absorption spectra of synthesized material show a red shift in the optical absorption on increase of S^{2-} ion concentration. Variation in electrical conductivity obtained from impedance measurements at different temperatures has been suitably correlated to Davis–Mott model.

✉ P. K. Shukla
    pks.vits@gmail.com

    Harit Kumar Sharma
    haritsharma2@gmail.com

    S. L. Agrawal
    sla_ssi1956@rediffmail.com

[1] SSI Laboratory, Department of Physics, APS University, Rewa, Madhya Pradesh 486003, India

[2] I.T.S Engineering College, Greater Noida, Uttar Pradesh 201308, India

1 Introduction

In recent times wide band gap II-VI semiconductors are reckoned as novel materials for development of optoelectronic devices owing to their unique optical and electrical properties. Among the different members of this group, ZnS has been extensively investigated as it has numerous application possibilities to its credit [1]. It is being considered as favourable exotic material for photoluminescent, electoluminescent and cathodoluminescent devices due to its superior chemical stability compared to other chalcogenides such as ZnSe [2].

Besides, it exhibits excellent optical transmission property with high refractive index of ~2.27 at 1 µm which makes it a prospective material for use in novel photonic crystal devices operating from visible to near infrared region [3]. ZnS crystal usually exhibit two structural polymorphs; one is cubic phase with a Zinc blende structure (c-ZnS) while the other is hexagonal phase with a wurtzite structure (h-ZnS) [4]. The cubic phase of Zinc Sulphide (c-ZnS) is more stable at low temperatures and transforms to less dense hexagonal wurtzite phase above 1035 °C [4]. After the emergence of nanotechnology nanocrystallites of ZnS have acquired much significance as one can obtain desirable physical property by controlling the size, morphology, and crystallinity of nanoparticles. The structural evolution of ZnS nanocrystallites, with particle size and their chemical environment have been the subject of investigation for the past decade or so. Since the inherent crystal structure of ZnS plays an important role in its physical and chemical properties, preparation of ZnS nano crystals with controllable phase is vital to develop them as building blocks in constructing the future nanoscale electronic devices [6]. The synthesis of ZnS remains a topic of interest for researchers and synthetic routes are being explored

to get a single phase material using economically and technically viable methods. Most of the researchers have used equal concentration of Zn^{2+} and S^{2-} precursors in the synthesis [7–11]. Though there have been some reports on the variation of $Zn^{2+}:S^{2-}$ ratio, the works are not substantive [12, 13]. In the present work we have done a systematic study on the effect of S^{2-} ion concentration in the synthesis of ZnS nanoparticles without using a capping agent. A simple chemical precipitation method with different molar ratio of precursor solution have been used to synthesize ZnS nanocrystal at room temperature and to analyze effect of S^{2-} ion concentration on the change in size and phase morphology of the ZnS nanoparticles.

2 Experimental details

The ZnS Nanoparticles have been prepared at room temperature without using any capping agent or surfactant via simple wet-chemical precipitation method. The starting materials used in the synthesis for ZnS nanostructures were Zinc(II) Chloride ($ZnCl_2$) and Sodium Sulphide (Na_2S) fused flakes. The chemical used in the synthesis were of analytical reagents (AR) grade and used without any further purification. For the synthesis, aqueous solutions of $ZnCl_2$ and Na_2S fused flakes were prepared separately and then required amount of later was mixed in the former drop wise under constant stirring at 700 rpm to obtain the desired molar ratios (viz., $Zn^{2+}:S^{2-}$ ratio of 1:0.5, 1:1, 1:3, 1:5, 1:7, 1:9). The chemical reaction involved in the synthesis of ZnS nanoparticles has been described elsewhere [13]. The stirring was continued for 50 min at room temperature to complete the reaction. Subsequently, precipitate was filtered out and rinsed with distilled water several times to remove the impurities. Finally, the products were allowed to dry up in an electrical oven at 150 °C for 10 h. The dried samples were allowed to cool down naturally at room temperature and grinded in an agate mortar to obtain ZnS nanopowder. The detail of samples prepared is summarized in Table 1. The crystallographic phases of ZnS nanopowder

Table 1 Details of ZnS samples synthesized with different molar ratio of Zn^{2+} & S^{2-} in precursor solution

Sample identification	Molar concentration ratio ($Zn^{2+}:S^{2-}$)	Calcinations temperature (°C)
HS$_1$	1:0.5	150
HS$_2$	1:1	150
HS$_3$	1:3	150
HS$_4$	1:5	150
HS$_5$	1:7	150
HS$_6$	1:9	150

were analysed using X-ray diffractogram (XRD) taken from Shimadzu (model XRD 6100) with CuKα radiation ($\lambda = 1.5406$ Å). Microstructural information was gathered with the help of Carl Ziess make environmental scanning electron microscope (SEM) (model EVO18). In order to investigate surface morphology and particle size atomic force microscopy (AFM) (SPM model AA 3000, Angstrom Advanced Ins, USA) was conducted. Electrical characterization of all synthesized ZnS samples were characterized by LCR meter (Hioki Japan 3520) in the frequency range (40 Hz–100 kHz) and temperature range (30–90 °C).

3 Results and discussions

3.1 Structural analysis

Figure 1 shows the XRD pattern of as synthesized ZnS powdered samples for HS$_1$–HS$_6$. The XRD diffraction patterns of sample HS$_1$ exhibit broad diffraction peaks at 2θ positions of ~28.6°, 47.98°, 56.62°. The peaks have been indexed with the JCPDS card no. 12-0688. In sample HS$_2$ the observed diffraction peaks at ~28.64°, 47.78°, and 56.52° matches very well with the wurtzite phase of ZnS crystal for their intensity and peak position. The observed peaks slightly shift towards lower Bragg angles as the concentration of sulphur is increased during synthesis. The diffraction peaks are significantly broadened essentially due to extremely small crystallite size. Rietveld full profile matching (online full profile matching developed by L. Lutterotti using COD) shows the presence of two phases: wurtzite ZnS and traces of insulating sulphur phase. On
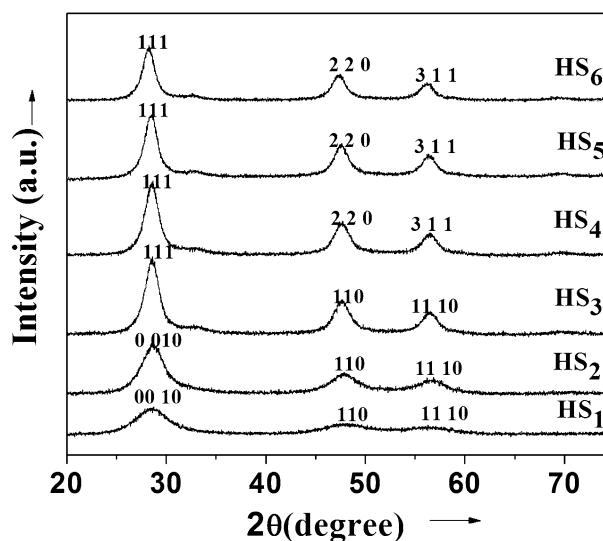

Fig. 1 XRD patterns of the ZnS nanoparticles synthesised with different molar ratio of $Zn^{2+}:S^{2-}$ in precursor solution

further increasing sulphur concentration in the precursor solution ($Zn^{2+}:S^{2-} = 1:3$, Sample HS_3), XRD peaks shift slightly towards lower angle with increase in peak intensity. Rietveld fit for sample HS_3 (Fig. 2b) suggests transformation of wurtzite phase to sphalerite phase of ZnS. It is indicated by existence of three phases namely sphalerite, wurtzite 8-H and wurtzite 10-H and in accordance with JCPDS card no. 05-0566, 72-0162, 72-0163. Refinement data of sample HS_4 (Fig. 2c) reveals the presence of only sphalerite phase matching closely with JCPDS Card no. 05-0566. The diffraction data for the samples obtained with higher S^{2-} ion concentrations in the precursor solution (HS_5 & HS_6) exhibit peaks corresponding to sphalerite phase (JCPDS Card No. 05-0566) and Retvield analysis confirms existence of only sphalerite phase in these samples. Thus, XRD analysis shows that initially at lower concentration of sulphur in the precursor solution, metastable wurtzite phase is formed even though the surface energies are more favourable for the sphalerite phase [14]. On increasing S^{2-} ion concentration both the phases nucleate simultaneously which transform to sphalerite phase of ZnS for $Zn^{2+}:S^{2-}$ ratio $\geq 1:5$ in the precursor solution. Therefore, availability of Zn^{2+} ions and S^{2-} ions as well as the coordination environment plays highly important role in the nucleation and growth kinetics of the two phases of ZnS nanocrystals.

The crystallite size corresponding to the observed ZnS peaks have been calculated using Debye–Scherer relation [15]

$$D = \frac{0.9\lambda}{\beta \cos \theta} \tag{1}$$

where λ = wave length of the X-ray used, β = full width at half maximum (FWHM) in radians, θ = Bragg angle, D = mean size of crystallites. The estimated crystallites size of the synthesized ZnS nanoparticles along with other details on X-ray diffraction peaks is listed in Table 2. From the table it is apparent that the crystallites size of the synthesized ZnS increases with increasing sulphur concentration.

3.2 Surface morphological studies

Figure 3 shows SEM micrographs for sample HS_2, HS_4, HS_6 respectively on the same magnification scale. SEM micrograph of sample HS_2 shows the presence of tiny agglomerated particles of nanometer size. The image of sample HS_4 exhibits presence of random shaped particles (viz., spherical or triangular). At higher S^{-2} ion concentration the nanoparticles are appearing to coalesce by forming a neck between the two particles. SEM images of as-synthesized ZnS powder shows the formation of nanoparticles
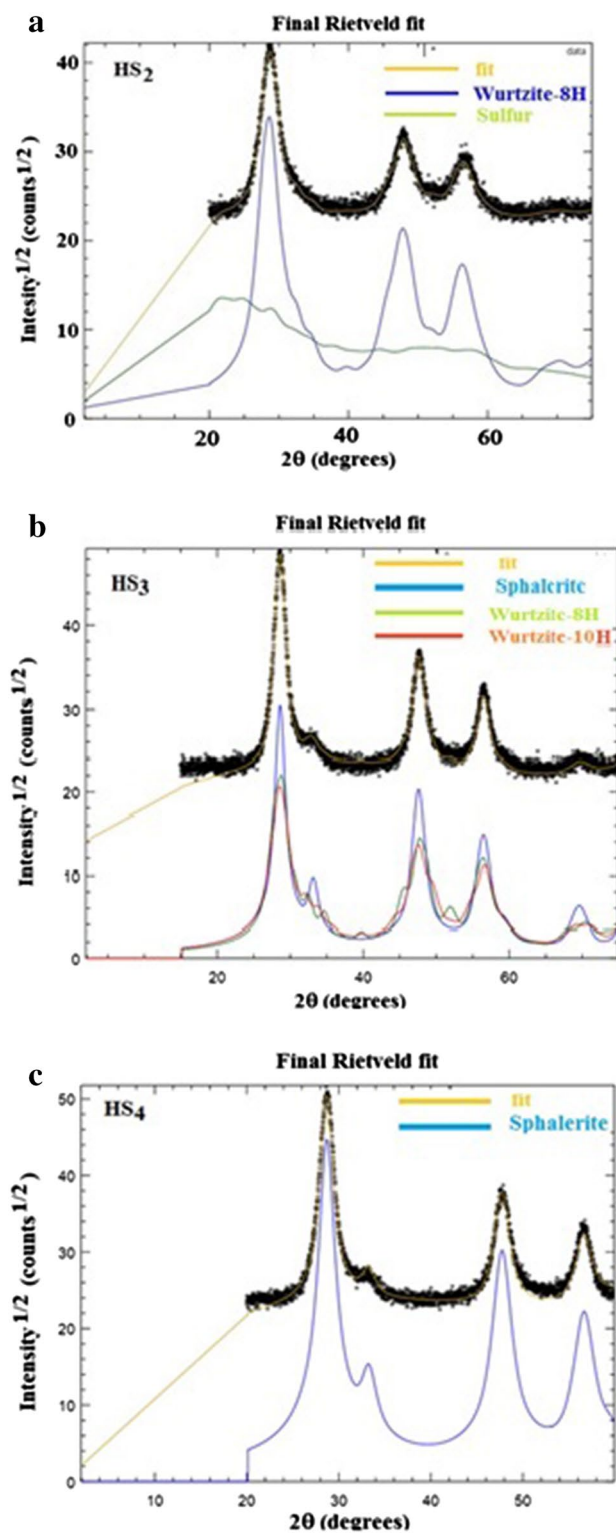

Fig. 2 Rietveld full profile matching for the ZnS nanoparticle samples **a** HS_2, **b** HS_3 and **c** HS_4

Table 2 XRD data of synthesised ZnS samples

Sample description	Angle (2θ)	d-spacing (Å)	Peak width (2θ in°)	Identified possible h k l planes	Crystal-lite size (nm)
HS$_1$ (Zn:S = 1:0.5)	28.60	3.12685	3.52600	0 0 10	2.32
	47.98	2.89520	1.98000	1 1 0	4.38
	56.62	1.89460	3.02000	1 1 10	2.98
HS$_2$ (Zn:S = 1:1)	28.64	3.11418	2.58140	0 0 10	3.17
	47.78	1.90203	2.81170	1 1 0	3.08
	56.52	1.62691	3.16000	1 1 10	2.85
HS$_3$ (Zn:S = 1:3)	28.56	3.12271	1.68960	1 1 1	4.84
	47.61	1.90833	1.90000	1 1 0	4.56
	56.45	1.62857	1.84500	1 1 10	4.88
HS$_4$ (Zn:S = 1:5)	28.53	3.12542	1.64130	1 1 1	4.99
	47.60	1.90877	1.87210	2 2 0	4.63
	56.43	1.62918	1.82860	3 1 1	4.92
HS$_5$ (Zn:S = 1:7)	28.45	3.13414	1.52890	1 1 1	5.35
	47.55	1.91052	1.65730	2 2 0	5.23
	56.37	1.63082	1.67500	3 1 1	5.37
HS$_6$ (Zn:S = 1:9)	28.23	3.15834	1.46860	1 1 1	5.57
	47.30	1.92001	1.62170	2 2 0	5.83
	56.14	1.63702	1.60000	3 1 1	5.62

The crystallite size is calculated using Debye–Scherer relation for the all the three broad peaks in XRD-pattern

Fig. 3 Scanning electron micrographs of the synthesized ZnS nanoparticles sample HS$_2$, HS$_4$, and HS$_6$
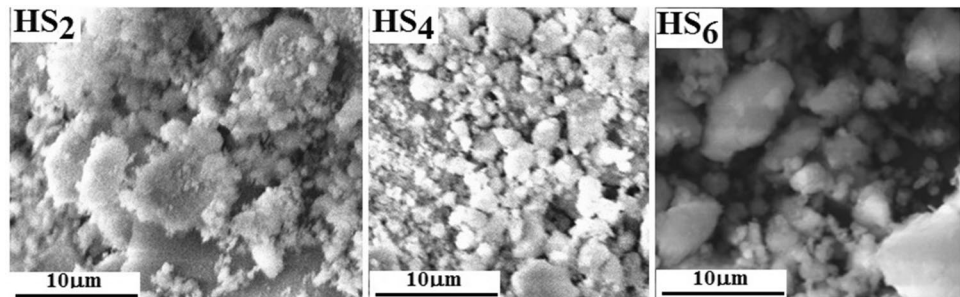
and particles size increases with increase of S^{2-} source concentration supporting XRD data.

Atomic force microscopy (AFM) allows us to get microscopic information about the surface structure and topographies representing the surface relief. This technique offers digital imaging which allow quantitative measurements of surface structures, such as root mean square roughness (Rq), or average roughness (Ra), and analysis of images with different perspectives, including three dimensional simulations [16, 17]. Here this technique has been used to visualize the surface relief and determine the effect of sulphur concentration on surface properties. Figure 4 illustrates two and three dimensional AFM images of the ZnS nanoparticles for different sulphur content. The AFM images clearly reveal formation of nanoparticles. From the two dimensional view of samples HS$_2$ and HS$_4$ it is noted that most of the particles are well separated and attached as grapes in a cluster and are spherical in shapes whereas the particles agglomerates and tend to coalesce to form bigger

particles at higher sulphur concentration. The size of particles is in the range of 10–100 nm. The 3D view revealed that the growth direction of particles is inhomogeneous. The surface roughness and average height of the ZnS nanoparticles for HS$_2$, HS$_4$, and HS$_6$ have been estimated from AFM image and listed in Table 3. It is important to note that the obtained values are averaged and there is a statistical variation associated with them, which depends on the location of the measurements performed on the samples [16, 17].

3.3 Optical studies (UV–vis absorption study)

Measurements on the optical absorption characteristics of ZnS nanoparticles was performed by dispersing a very small amount of the powder in distilled water, contained in quartz cavetti. The appearance of characteristic absorption due to ZnS nanoparticles lies in the wavelength range of 200–340 nm. Absorption characteristics of samples were

Fig. 4 Atomic force micrographs of the synthesized ZnS nanoparticles samples HS$_2$, HS$_4$, HS$_6$
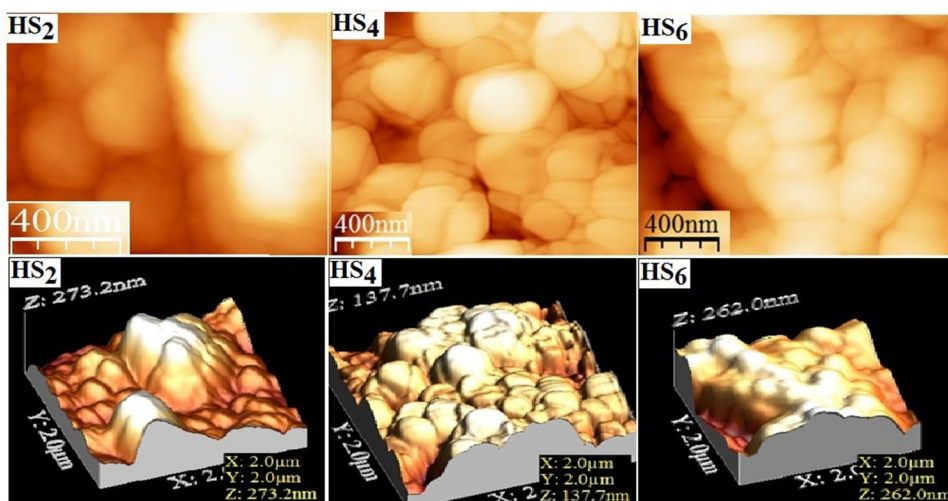

Table 3 Roughness and average height of the ZnS nanoparticles obtained from AFM analysis

Sample description	Average roughness (nm)	R M S roughness (nm)	Average hight (nm)
HS$_2$	46.27	58.71	185.58
HS$_4$	18.06	22.56	79.23
HS$_6$	37.15	47.39	164.60

obtained by measuring the absorbance (A) at different wavelength (λ) and there after calculating the absorption coefficient (α) at corresponding wavelengths using well known Beer–Lambert's relation:

$$\alpha = \frac{2.303A}{d} \tag{2}$$

where, d is the path length. The incident photon energy (hv), absorption coefficient (α) and band gap (E$_g$) of the material are inter related by the well-known Tauc relation [18].

$$\alpha h\nu = K(h\nu - E_g)^n \tag{3}$$

where K is the edge width parameter, n depends on the type of transition, i.e. allowed direct, allowed indirect, forbidden direct and forbidden indirect for which it can have value of 1/2, 2, 3/2, and 3 respectively. The direct optical band gap values of ZnS nanoparticles have been determined by plotting a graph between $(\alpha h\nu)^2$ versus hv (Fig. 5) and extrapolating the straight line portion of the graph to the hv axis (showing the maximum transmission, i.e. $\alpha = 0$). The so obtained energy band gap values have been shown in Table 4. Moreover, Fig. 5 shows that band gap of ZnS nanoparticles decreases for samples synthesized with increasing S^{2-} concentration in the precursor solution. This is possibly due to the change in phase morphology and size of
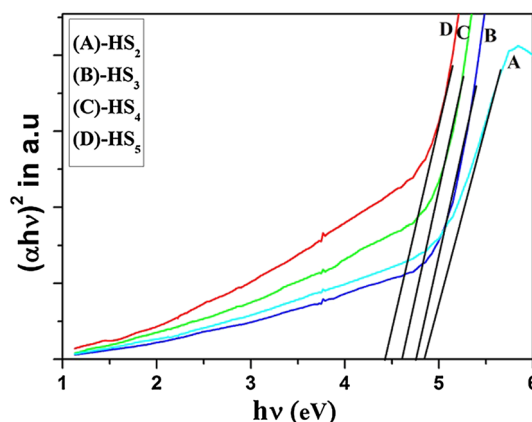

Fig. 5 Tauc's plot for the determination of optical band gap for samples HS$_2$ (*A*), HS$_3$ (*B*), HS$_4$ (*C*) and HS$_5$ (*D*)

Table 4 Optical band gap of ZnS samples obtained using Tauc's plot of UV–Vis data

Sample description	Optical band gap (eV)
HS$_2$ (A)	4.85
HS$_3$ (B)	4.75
HS$_4$ (C)	4.65
HS$_5$ (D)	4.59

ZnS nanoparticles as discussed above in Sects. 3.1 and 3.2. The red shift of band gap essentially occurs due to growth of grains and decrease in defect states near the band edges.

3.4 Electrical conductivity study

Since in disordered systems the temperature dependence of DC conductivity is a resonant process by which

electron or hole transfer takes place, the dc conductivity depends sensitively on the activation energy of the most prominent current paths. The current paths carrying most of the current may be different for different temperatures, thereby altering the temperature dependence of conductivity. Thus, the temperature dependence of conductivity contains lot of information about the charge transport mechanism. In the present study, the observed conductivity behaviour of as synthesized ZnS nanoparticles samples can be best described by VRH model [19–22]. According to this model, the standard energy band scheme describing a crystalline material changes in the amorphous/disordered case so that the valence and the conduction bands stretch out and develop a tail while a middle allowed band (compensated levels) also approaches the centre of forbidden band gap. Carriers possessing energies within the tails and the central band are described by localized states while for other energies, the carriers lie in the extended states. In the VRH model, there are three mechanisms of charge transport with each dominating in different temperature ranges:

i. At the highest temperatures, the carriers are excited into extended states where they acquire mobilities orders of magnitude greater than in the localized states;
ii. In the medium temperature regime, the carriers are excited into localized states in the valance and conduction band tails; and
iii. At low temperatures, conduction occurs by tunneling between states located in the central band near the Fermi level (variable range hopping).

In case (i) the temperature dependence of conductivity $\sigma_{DC\,(T)}$ exhibits Arrhenius behaviour with activation energy that is equal to the difference between the Fermi level and the energy that defines the boundary between localized and extended states; In case (ii), electrical conduction occurs by thermally activated hopping and $\sigma_{DC(T)}$ still follows Arrhenius behaviour but with different activation energy involving Fermi level energy, the energies of tail edges, and hopping activation energy and there pre-exponential factor acquires weak temperature dependence. Finally, for case (iii), conduction is associated with phonon-assisted tunnelling also known as "variable-range hopping" and in this case $\sigma_{DC(T)}$ can be expressed as

$$\sigma_{DC} = \sigma_0 \exp\left(-\frac{T_0}{T}\right)^x \qquad (4)$$

where the characteristic temperature (T_0) and the pre-exponential factor (σ_0) are related to the localization length and density of states and x is an arbitrary fitting parameter given as x = 1/(n + 1). Here n is the

dimensionality factor having values 1, 2 and 3 for the one, two and three dimensional hopping of charge carriers respectively [21–24]. Electrical conductivity of the samples with $Zn^{2+}:S^{2-}$ ratio 1:1, 1:5 and 1:9 have been calculated for different temperatures. The goodness of best fit parameter (R^2 values) calculated from linear fit lines for fitting parameter x = 1/2, 2/3 and 1/4 showed that temperature dependence of conductivity is best described with fitting parameter x = 1/4 in the present system. Variation of conductivity with temperature for x = 1/4 is shown in Fig. 6. The characteristic temperature T_0 extracted from the linear fit lines is listed in Table 5. On further exploring the behaviour it is also observed that the variation in conductivity exhibits three different linear regions ($R^2 \approx 1$) on the temperature scale. At lower temperatures (308°K to 328°K) VRH scheme dominates while with increasing temperature (temperature range 328–363 K) the conductivity shows a transition from ES-VRH (extended state-VRH) to Mott-VRH which results from the thermal closing of the coulombic gap. Thus, the present analysis indicates that the conductivity response of ZnS nanoparticles can be best described by Mott-VRH, model in the temperature range 300–360 K.
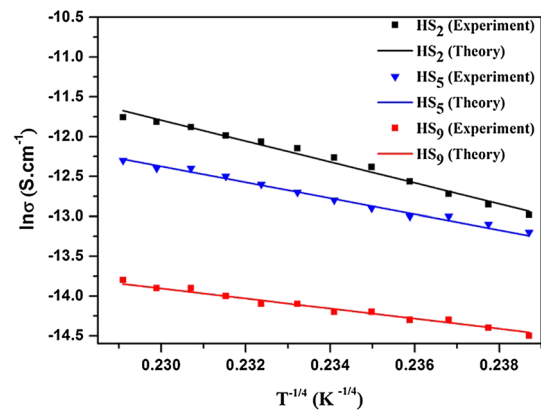

Fig. 6 Temperature dependence of electrical conductivity fitted to Mott-VRH model for samples HS_2, HS_2, HS_5 and HS_9

Table 5 Goodness of fit parameter (R^2) and characteristic temperature (T_0) obtained from linear fit lines in Mott-VRH model with fitting parameter x = 1/4

Sample	R² value	T₀ (K)
HS_2	0.9846	3.46×10^8
HS_4	0.9984	9.9×10^7
HS_6	0.9993	1.8×10^7

4 Conclusion

It is possible to synthesise ZnS nanoparticles with wurtzite hexagonal phase and sphalarite phase by simply changing molar concentrations of Zn^{2+} and S^{2-} in the precursor solution and without using any capping agent. XRD data and AFM measurements show the formation of nanoparticles of different phase and morphology. Retvield analysis of XRD data have confirmed that wurtzite phase converts to sphalarite phase of ZnS with increasing S^{2-} concentration in the precursor solution. SEM image shows microcrystalline behaviour of ZnS samples with of tiny agglomerated particles of nanometer size which are appearing to coalesce at higher S^{-2} ion concentration. The optical band gap result corresponds to the reported values for the phase structure of the synthesized samples. It is observed that the optical band gap energy for the samples decreases with increase of sulphur ion concentration in the precursor solution. This is either related to large size of the dislocation or changing barrier height because of variation in grain size in the nanoparticles. The decrease in energy band gap for increasing sulphur content is also attributed to improvement in the crystallinity as supported by the XRD studies. The temperature dependence of electrical conductivity is found to be better described by Mott-Davis model for disordered semiconductors.

References

1. X. wang, H. Huang, B. Liang, Z. Liu, D. Chen, G. Shen, ZnS nanostructures: synthesis, properties and applications. Crit. Rev. Solid State Mater. Sci. **38**(1), 57–90 (2013)
2. K.S. Rathore, D. Patidar, Y. Janu, N.S. Saxena, K. Sharma, T.P. Sharma, Structural and optical characterization of chemically synthesized ZnS nanoparticles. Chalcognide Lett. **5**, 105–110 (2008)
3. W. Park, J.S. King, C.W. Neff, C. Liddell, C.J. Summers, ZnS based photonic crystals. Phys. Status Solidi **229**, 949–960 (2002)
4. B. Gillbert, B.H. Frazer, H. Zhang, F. Huang, J.F. Banfield, D. Haskel, J.C. Lang, X-ray absorption spectroscopy of the cubic and hexagonal poly type ZnS". Phys. Rev. B **66**, 245205 (2002)
5. S.B. Qadri, E.F. Sketton, "The effect of particle size on the structural transition in Zinc Sulphide". J. Appl. Phy **89**, 115–119 (2001)
6. S.D. Esgreniers, L. Beaulieu, I. Lepage, "Pressure-induced structural changes in ZnS". Phys. Rev. B **61**, 8726–8733 (2000)
7. J.F. Suyver, S.F. Weister, J.J. Kelly, A. Meijerink, Synthesis and photoluminescence of nanocrystallite ZnS. Nano Lett. **1**, 429 (2001)
8. X. Fang, T. Zhai, U. K. Gautam, L. Li, L. Wu, Y. Bando, D. Golberg, ZnS nanostructures: from synthesis to applications. Prog. Mater. Sci. **56**,175–287 (2011)
9. Y. Ding, X.D. Wang, L.Z. Wang, Phase controlled synthesis of ZnS nanobelts: zinc blende vs wurtzite. Chem. Phys. Lett. **398**, 32–36 (2004)
10. A. Marusamy, S. Agilan, M. Kumarsamy, C.K. Senthil kumaran, M. Sarvanakumar, The influence of the Zn/S source concentration ratio on its structural, optical and magnetic properties of ZnS quantum dots. Chalcogenide Lett. **10**, 179–187 (2003)
11. H.K. Sharma, P.K. Shukla, L.S. Agrawal. Structural and electrical studies on ZnS nanoparticles prepared without using capping agent. J. Optoelectron. Adv. Mater. **17**, 608–613 (2015)
12. C.C. Yang, S. Li, Size, dimensionality and constituent stoichiometry dependence of bandgap energies in semiconductor quantum dots and wires. Phys. Chem. C **112**, 2851 (2008)
13. P.C. Patel, N. Srivastav, C.P. Srivastav, Synthesis of wurtzite ZnS nanocrystallites at low temperature. J. Mater. Sci. **13**, 1367 (2013)
14. F.A. La Porta, J. Andre´s, M.S. Li, J.R. Sambrano, J.A. Varelaa, E. Longoa, Zinc blende versus wurtzite ZnS nanoparticles: control of the phase and optical properties by tetrabutylammonium hydroxide. Phys. Chem. Chem. Phys. **16**, 20127 (2014)
15. B.D. Culty, *Elements of X-ray Diffraction*, 2nd edn. (Addision Wesley company, USA, 1956), p. 102
16. G. Nabiyouni, R. Sahraei, M. Toghiany, M. Majles, K. Hedayati, Preparation and characterization of nanostructured ZnS thin film grown on glass and N-type Si substrate using a new chemical bath deposition. Adv. Mater. Sci. **27**, 52–57 (2011)
17. M.A. Martinz, C. Guillen, J. Herrero, Cadmium sulphide growth investigations on different SnO_2 substrates. Appl. Surf. Sci. **140**, 182–189 (1999)
18. D.A. Skoog, F. Holler, C. James, R. Stanley, *Principles of Instrumental Analysis*, 6th edn. (Thomson Brooks, Cole, Belmont, CA, 2007), pp. 169–173
19. P. Nagels, *Topics in Applied Physics, Amorphous Semiconductors*, ed. by M.H. Brodsky (Springer, New York, 1979)
20. N.F. Mott, E.A. Davis, Electronic Processes in Non-Crystalline Materials, (Clareendon, Oxford University Press, New York, 1979)
21. M.A. Majeed Khan, S. Kumar, M. Alhoshan, A.S. Aidwayyan, Spray pyrolysed Cu_2ZnSnS_4 absorbing layer: a potential candidate for photovoltaic applications. Opt. Laser Technol. **49**, 196–201 (2013)
22. Y. Tian, H. Lu, J. Tian, C. Li, C. Hui, X. Shi, Y. Huang, C. Shen, H. Gao, Influence of Si Co-doping on electrical transport properties of magnesium doped boron nanoswords. Appl. Phys. Lett. **100**, 103112 (2012)
23. W.J. Lu, B.C. Zhao, R. Ang, W.H. Song, P.Y. Sun Studies of electrical and thermal transport properties of the electron-doped manganite Sr0.9Ce0.1MnO3. Phys. B **367**, 243–248 (2005)
24. O.S. Panwar, I. Rawal, R.K. Tripathi, A.K. Srivastava, M. Kumar, Structural, nanomechanical and variable range hopping conduction behavior of nanocrystalline carbon thin films deposited by the ambient environment assisted filtered cathodic jet carbon arc technique. J. Alloys Compd. **628**, 135–145 (2015)